Science Advances

AAAS

advances.sciencemag.org/cgi/content/full/4/6/eaat1513/DC1

Supplementary Materials for

Geomorphic expression of rapid Holocene silicic magma reservoir growth beneath Laguna del Maule, Chile

Brad S. Singer, Hélène Le Mével, Joseph M. Licciardi, Loreto Córdova, Basil Tikoff, Nicolas Garibaldi, Nathan L. Andersen, Angela K. Diefenbach, Kurt L. Feigl

Published 27 June 2018, *Sci. Adv.* **4**, eaat1513 (2018)
DOI: 10.1126/sciadv.aat1513

This PDF file includes:

Sample information and data for cosmogenic ^{36}Cl measurements and exposure ages.

table S1A. Data from cosmogenic ^{36}Cl dating samples. Properties and analytical data for samples analyzed for cosmogenic ^{36}Cl. Altitudes, latitudes, and longitudes were determined with GPS and from the 1 meter-resolution Digital Elevation Model (DEM). The rock dissolved indicates the amount processed for AgCl extraction chemistry. The ^{37}Cl carrier is from Oak Ridge National Laboratory and has a ^{37}Cl enrichment of 98.21%. Uncertainties on ^{35}Cl/^{37}Cl and ^{36}Cl/^{37}Cl ratios and exposure ages represent propagated 1σ analytical/internal uncertainties only. In the main text, we report the exposure ages with the 2σ internal uncertainties. Sample ^{36}Cl concentrations are corrected for ^{36}Cl contributed by blanks. Exposure age uncertainties in parentheses incorporate external uncertainties, including production rate uncertainties; comparisons of the ^{36}Cl ages with those derived from independent chronometers (e.g., ^{40}Ar/^{39}Ar) must take into account these external uncertainties. Ages "w/erosion" are calculated with a prescribed rock surface erosion rate of 5 mm/kyr, and ages "w/water" are calculated with a prescribed 0.5 fraction of pore water content; these ages are included for sensitivity purposes.

Sample	Lat. (°S)	Lon. (°W)	Elev. (m)	Thick. (cm)	Density (g/cm)	Shielding	Rock diss. (g)	^{37}Cl carrier (mg)	^{35}Cl/^{37}Cl (±1σ)	^{36}Cl/^{37}Cl (e^{-15}, ±1σ)	^{36}Cl conc. (e^{4} at/g, ±1σ)	Exposure Age (ka, ±1σ)	Age w/erosion (ka, ±1σ)	Age w/water (ka, ±1σ)
15-SLM-05	-36.02584	-70.47631	2376	3.00	2.60	0.9989	20.0690	0.887	0.391 ± 0.004	885.4 ± 12.9	68.71 ± 1.04	**9.4 ± 0.2 (0.7)**	9.7 ± 0.2 (0.8)	9.5 ± 0.2 (0.7)
SLM-15-13	-35.99669	-70.44640	2386	2.00	2.60	0.9919	20.2219	0.882	1.177 ± 0.002	361.8 ± 6.8	38.58 ± 0.75	**8.8 ± 0.3 (1.0)**	8.4 ± 0.3 (0.9)	10.3 ± 0.3 (0.9)
LDM-15-21	-36.06629	-70.57440	2446	3.00	2.60	0.9988	19.9975	0.887	2.623 ± 0.033	500.8 ± 8.1	208.93 ± 3.38	**8.4 ± 0.6 (1.9)**	7.5 ± 0.4 (1.5)	12.7 ± 0.4 (2.4)
SLM-16-27	-36.03074	-70.49751	2388	1.75	2.60	0.9884	20.0774	0.882	2.379 ± 0.014	365.1 ± 8.2	102.34 ± 2.29	**6.6 ± 0.3 (1.0)**	6.1 ± 0.3 (0.8)	9.9 ± 0.4 (1.8)
SLM-16-28	-36.02160	-70.48003	2382	2.00	2.60	0.9840	20.1295	0.887	0.585 ± 0.004	535.8 ± 11.7	45.03 ± 1.00	**7.5 ± 0.2 (0.5)**	7.6 ± 0.2 (0.5)	7.7 ± 0.2 (0.5)
SLM-16-29	-36.02491	-70.47676	2374	1.75	2.60	0.9943	20.1973	0.887	0.597 ± 0.006	347.1 ± 8.2	28.65 ± 0.70	**4.2 ± 0.1 (0.3)**	4.2 ± 0.1 (0.3)	4.3 ± 0.1 (0.3)
SLM-16-30	-36.05515	-70.44004	2520	2.00	2.60	0.9934	20.0551	0.890	2.858 ± 0.019	193.0 ± 4.4	150.97 ± 3.45	**0.8 ± 0.3 (0.3)**	0.7 ± 0.3 (0.4)	3.4 ± 0.3 (0.8)
SLM-16-31	-36.17836	-70.47636	2550	2.75	2.60	0.9913	20.1207	0.886	2.771 ± 0.011	257.7 ± 5.2	151.83 ± 3.08	**2.5 ± 0.4 (0.6)**	2.4 ± 0.3 (0.7)	5.3 ± 0.3 (0.9)
SLM-16-32	-36.19862	-70.43153	2447	2.00	2.60	0.9956	20.0729	0.885	2.868 ± 0.019	207.6 ± 7.0	168.05 ± 5.71	**1.4 ± 0.3 (0.4)**	1.3 ± 0.2 (0.3)	4.3 ± 0.3 (0.9)
CLBLK-12	--	--	--	--	--	--	--	0.894	0.028 ± 0.001	44.7 ± 4.1	--	--		
CLBLK-15	--	--	--	--	--	--	--	0.892	0.236 ± 0.000	19.9 ± 2.5	--	--		

table S1B. Major element compositions of cosmogenic ^{36}Cl dating samples. Major element chemistry of samples analyzed for cosmogenic ^{36}Cl. All major element chemistry and LOI is listed in weight percent and was performed with X-ray fluorescence with 0.01% detection limit. H_2O and CO_2 were each assumed to account for half of the LOI signal.

Sample	SiO_2	TiO_2	Al_2O_3	Fe_2O_3	MnO	MgO	CaO	Na_2O	K_2O	P_2O_5	Cr_2O_3	LOI
15-SLM-05	69.70	0.34	14.30	1.89	0.01	0.12	0.05	0.68	11.20	0.07	<0.01	1.25
SLM-15-13	64.00	0.95	16.80	6.42	0.09	1.01	3.71	4.44	2.88	0.11	<0.01	0.95
LDM-15-21	70.00	0.39	14.80	2.51	0.07	0.58	1.83	4.59	3.78	0.07	0.02	0.86
SLM-16-27	69.40	0.46	15.90	2.50	0.02	0.13	1.37	4.75	4.17	0.05	0.02	0.94
SLM-16-28	71.00	0.46	14.30	2.48	0.04	0.27	0.28	1.92	8.71	0.08	0.02	1.53
SLM-16-29	70.90	0.36	15.00	1.19	0.02	0.15	0.12	1.15	10.80	0.06	0.01	0.88
SLM-16-30	73.80	0.25	14.30	1.56	0.08	0.26	0.91	4.87	4.00	0.04	0.01	0.51
SLM-16-31	74.10	0.23	14.10	1.40	0.07	0.19	0.85	4.72	3.99	0.04	0.03	1.38
SLM-16-32	73.90	0.25	14.30	1.43	0.07	0.26	0.94	4.74	3.96	0.06	0.01	1.37

table S1C. Trace element compositions of cosmogenic ^{36}Cl dating samples. Trace element chemistry of samples analyzed for cosmogenic ^{36}Cl in ppm. Cl is calculated using isotope dilution based on AMS data. Trace elements were analyzed by ICP-MS with detection limits (ppm) as follows: 10 for B, Cr, Li; 0.1 for Sm, Th; 0.05 for Gd, U.

Sample	Rock type/setting	Cl (±1σ)	B	Sm	Gd	U	Th	Cr	Li
15-SLM-05	990 ka Bobadilla tuff/shoreline bench	22.9 ± 0.3	<10	3.1	2.84	4.35	16.3	71	16
SLM-15-13	1.01 Ma Andesite of Volcan La Zorra andesite/shoreline bench	88.0 ± 0.3	<10	4.0	3.93	3.18	10.4	58	<10
LDM-15-21	Rhyodacite of Colada Dendriforme (*rdcd*)	890 ± 75	35	3.2	2.43	5.52	19.9	113	31
SLM-16-27	990 ka Bobadilla tuff/shoreline bench	527 ± 14	18	5.2	4.50	4.43	16.3	143	17
SLM-16-28	990 ka Bobadilla tuff/shoreline bench	25.3 ± 0.3	<10	1.7	1.83	3.40	13.2	89	<10
SLM-16-29	990 ka Bobadilla tuff/shoreline bench	26.2 ± 0.5	<10	6.1	5.84	4.36	16.4	61	15
SLM-16-30	Younger Rhyolite of Cari Launa (*rcl*)	1806 ± 155	18	4.0	3.13	5.40	20.0	92	34
SLM-16-31	Rhyolite of Barrancas complex (*rcb*)	1313 ± 47	18	3.9	3.19	5.36	19.9	167	33
SLM-16-32	Rhyolite of Barrancas complex (*rcb*)	1874 ± 163	22	4.1	3.19	5.30	19.5	87	34

Geodetic data and mapping of highstand paleoshoreline.

The 64 static GPS measurements are listed in Table S2. These GPS positions are compared to the values extracted from the 1 m resolution DEM. Figure S1 represents all the paleoshoreline surfaces identified in the field and mapped using the 1m resolution DEM. Colorscale shows the interpolated DEM elevations and circles are the 64 GPS points surveyed in 2014, 2015, and 2016. The map insets in fig. S1 B, C, and D: (1) confirm that the GPS sites chosen rest on the highstand paleoshoreline surface, and (2) estimate uncertainty of the GPS points based on the relative location within one outcrop surface. Most surfaces are inclined because they are covered by pumice lapilli and ash hence the main uncertainty in the GPS measurements comes from choice of the GPS site location within one mapped outcrop. Examination of each outcrop reveals that the positioning was relatively consistent and most GPS sites were chosen in the middle of the slope or at the higher point (break in slope). We checked that the heights relative to the WGS84 ellipsoid were consistent between the DEM and the GPS field measurements. The mean difference between the height from the DEM and the GPS measurement is 0.27 m. The standard deviation is 1.07 m. 25 out of 64 points agree within 1 cm (fig. S2). The minimum and maximum difference is 0.19 m and 2.6 m respectively. Based on these observations we attribute a total uncertainty for each GPS point of ±3 m (mostly reflecting uncertainty as to whether the measurement is from the mid-point across the surface or at the top/bottom of the surface).

table S2. Static GPS measurements of highstand paleoshoreline. Sixty-four static GPS measurements of Laguna del Maule paleo-highstand shoreline.

Longitude	Latitude	Elevation (m)
-70.56995	-36.10235	2366.5
-70.57587	-36.03336	2369.1
-70.57638	-36.10091	2370.1
-70.58743	-36.08229	2370.7
-70.57554	-36.03362	2371.5
-70.58984	-36.09711	2371.8
-70.58460	-36.03498	2372.7
-70.46780	-36.00571	2373.7
-70.56628	-36.06806	2375.3
-70.58313	-36.03208	2375.5
-70.45047	-36.01351	2375.6
-70.49761	-36.03065	2375.6
-70.56471	-36.07575	2376.1
-70.57492	-36.06966	2376.2
-70.56706	-36.06369	2376.3
-70.47637	-36.02548	2376.6
-70.53518	-36.01882	2377.0
-70.56269	-36.01263	2377.3
-70.53997	-36.01899	2377.7
-70.47684	-36.01633	2377.8
-70.59764	-36.09537	2377.9
-70.48565	-36.01137	2378.4
-70.59894	-36.09090	2378.5
-70.54092	-36.01905	2378.5
-70.53236	-36.01801	2378.7
-70.47869	-36.01876	2381.7
-70.47995	-36.02153	2381.7
-70.56069	-36.10173	2381.8
-70.52228	-36.01650	2382.7
-70.49390	-36.02868	2382.9
-70.47223	-36.02400	2383.0
-70.44638	-35.99663	2385.5
-70.52179	-36.01704	2386.6
-70.54480	-36.10299	2387.2
-70.45604	-36.04417	2387.3
-70.49759	-36.03117	2387.5
-70.45330	-36.04004	2388.2
-70.47552	-36.02332	2388.7
-70.55334	-36.10109	2389.0
-70.45502	-36.04277	2389.5
-70.55654	-36.10062	2389.6
-70.45815	-36.04731	2390.5
-70.45314	-36.04795	2392.2
-70.45305	-36.05530	2393.1
-70.45238	-36.04956	2393.7
-70.45228	-36.05169	2394.3
-70.45339	-36.06448	2395.6
-70.44821	-36.06382	2399.8
-70.45184	-36.06463	2401.1
-70.45350	-36.08134	2407.1
-70.45055	-36.07785	2407.8
-70.44708	-36.07404	2408.7
-70.45664	-36.08984	2410.4
-70.45537	-36.08523	2410.6
-70.44289	-36.12605	2413.0
-70.44298	-36.12689	2415.9
-70.45774	-36.09552	2419.0
-70.49581	-36.11794	2419.3
-70.50717	-36.10887	2419.6
-70.49433	-36.11867	2419.7
-70.44239	-36.12629	2419.9
-70.45816	-36.09729	2420.1
-70.50349	-36.11080	2422.7
-70.51059	-36.11037	2427.9

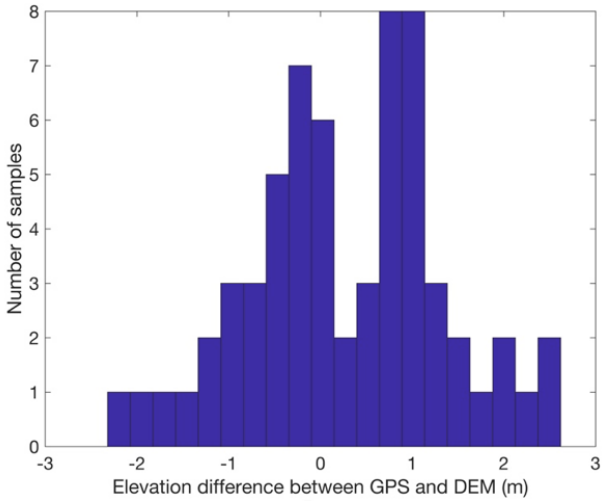

fig. S1. One-meter-resolution DEM and identification of highstand paleoshoreline outcrops. Histogram of elevation differences calculated between interpolated 1m DEM derived from photogrammetry and GPS field measurements at 64 points.

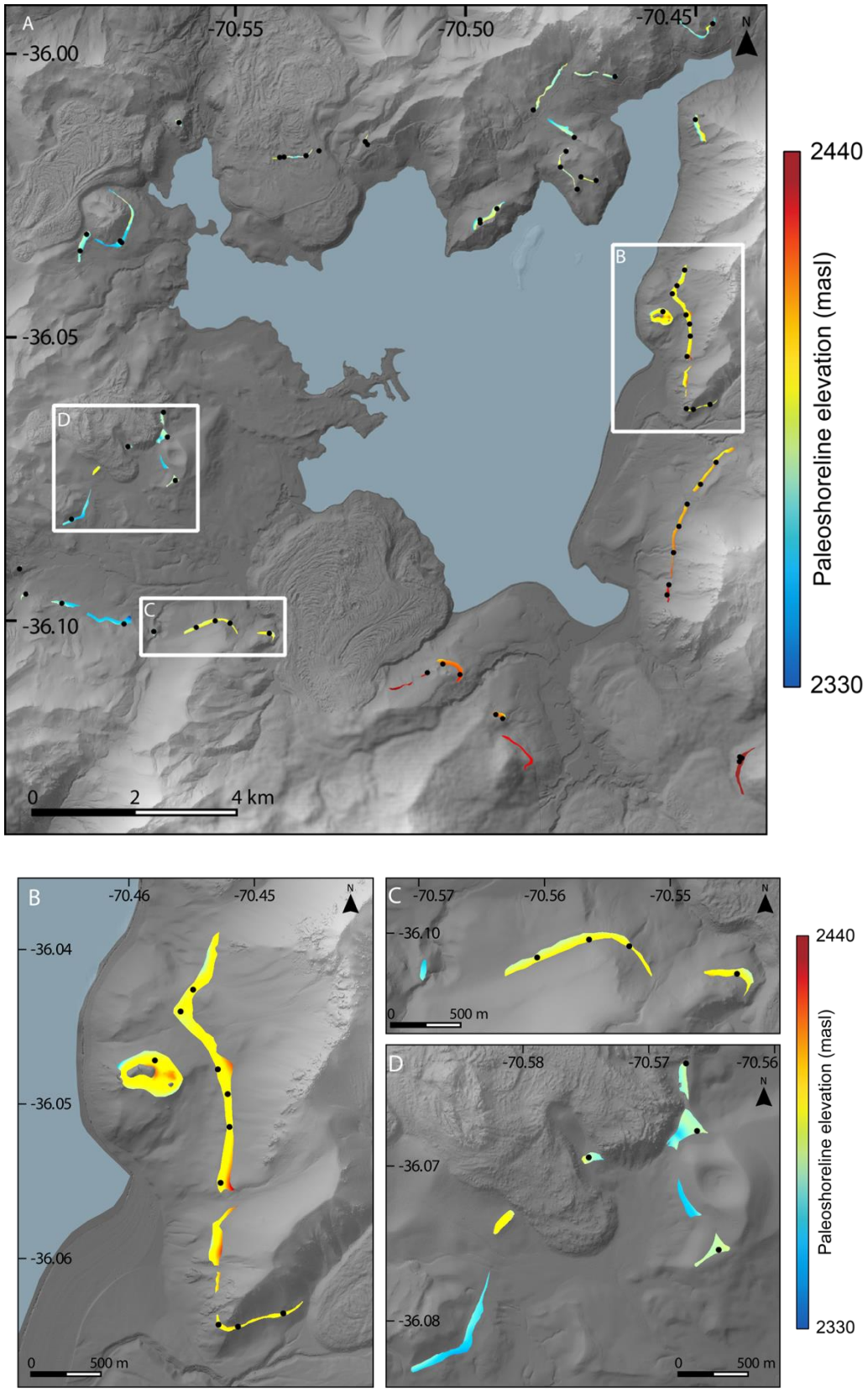

fig. S2. Histogram of elevation differences between GPS and DEM. (**A**) Highstand paleo-shoreline outcrop surfaces (colored polygons) mapped onto 1-meter resolution DEM. Location of 64 GPS measure-ments are black dots. Insets with details of selected areas are illustrated in panels (**B**, **C**, and **D**). Panel D illustrates an area where the highstand paleoshoreline is overlain by the 8.4 ka Colada Dendriforme rhyodacite (Fig. 3D in the main text).

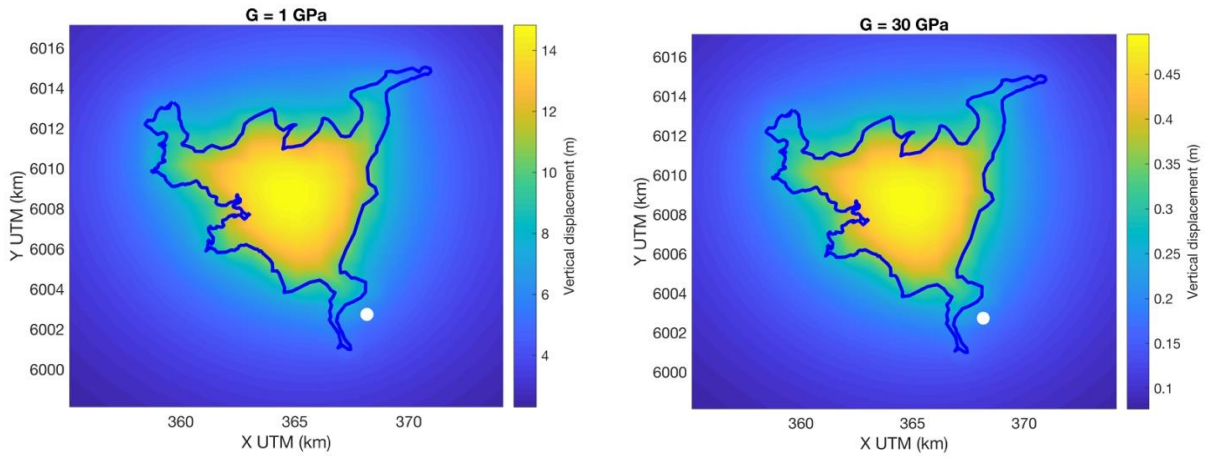

fig. S3. Estimated vertical displacement in response to crustal unloading from lake draining. Vertical displacement due to 200 m lake level drop for two values of crustal shear modulus: 1 GPa (left panel), and 30 GPa (right panel) using loading equations from (*65*) for an elastic crust. Contour of the lake as observed in 2012 (blue line). The unloading process is discarded as the cause of the observed paleoshoreline deformation (Fig. 4) based on the different location, spatial wavelength, and magnitude of the resulting surface displacement pattern. The white circle shows the position of the inferred source of inflation from our magma intrusion model.

Map and features associated with the trace of the Troncoso fault.

The gradual southeasterly increase in elevation of the highstand paleoshoreline is locally disrupted by a 20 m change in elevation across a regional NE-oriented lineament (fig. S4). Independent field observations near the lake and in the Troncoso canyon indicate that the lineament is the NE-striking, NW-dipping Troncoso fault. Well-defined geomorphic features (triangular facets, fig. S4, A & B) and discrete slip surfaces on the southeast flank of the Troncoso canyon, suggest that the Troncoso fault has accommodated tens of meters of normal dip-slip and some oblique-slip offsets. Although examination of InSAR satellite data indicates that the Troncoso fault has been inactive during the last decade, the Troncoso fault has experienced important northwest-side-down motions during the past ~10 kyr evinced by the 20 m offset in the paleoshoreline highstand surface. We interpret that the Troncoso fault may be partly accommodating strain associated with uplift caused by Late Holocene magmatic injection beneath the Barrancas complex, on the southeast end of the lake. There is no evidence that the Troncoso fault extends across the lake and is expressed in outcrops northeast of the lake, however the number of GPS stations is limited in this area.

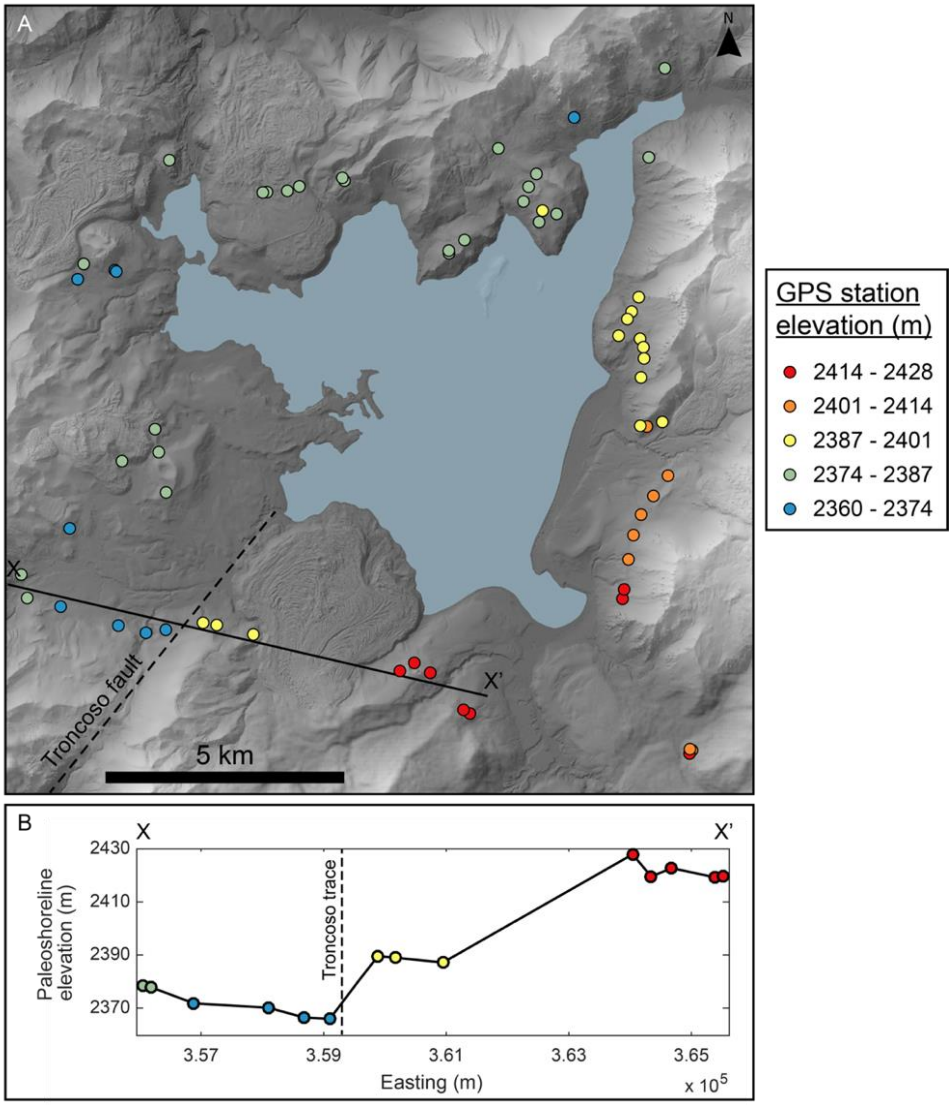

fig. S4. Map of highstand paleoshoreline surface where it intersects the trace of the Troncoso fault. (**A**) Hillshaded 1-meter resolution DEM of the Laguna del Maule volcanic field showing 64 static GPS stations (color coded for elevation) on the highstand paleoshoreline. (**B**) Transect X-X' illustrates the elevation change across the inferred trace of the northeast striking Troncoso fault.